Supporting Information

Enzymatic Degradation of DNA Probed by *In Situ* X-Ray Scattering

Kurinji Krishnamoorthy,[†,⊥] Sumit Kewalramani,[‡,⊥] Ali Ehlen,[†] Liane M. Moreau,[‡] Chad A. Mirkin,[*,‡,§] Monica Olvera de la Cruz,[*,†,‡,§,∥] Michael J. Bedzyk[*,†,‡,∥]

[†]Applied Physics Program, [‡]Department of Materials Science and Engineering, [§]Department of Chemistry and [∥]Department of Physics and Astronomy, Northwestern University, Evanston, Illinois 60208, United States.

[⊥] *These authors contributed equally to the work.*

[*] *Address correspondence to: bedzyk@northwestern.edu; m-olvera@northwestern.edu; chadnano@northwestern.edu*

S1. SAXS from pure DNase I

SAXS Intensity profiles were collected from DNase I dispersed in the enzyme buffer at a final concentration of 0.005 mg/ml (166.6 nM), which is the highest DNase I concentration used in our X-ray studies. The resultant background (solvent) subtracted intensity profile is shown in Fig. S1A. The SAXS profile from DNase I does not show any appreciable intensity modulations. Fig. S1B shows a comparison of the SAXS intensity profiles collected from pure water, reaction buffer and DNase I suspended in the reaction buffer corrected for scattering from the empty capillary. Overall, Figs S1A-B show that for q > 0.3 nm^{-1}, where intensity modulations due to Pro-SNA structure are observed (Fig. 1B), the DNase I scattering contributes only a featureless background. For appropriate background subtraction, the intensity profile collected from DNase I dispersed in the reaction buffer was subtracted out from the intensity profiles for the ProSNA-DNase I mixture systems (Figs. 1B, 2A, 4D).

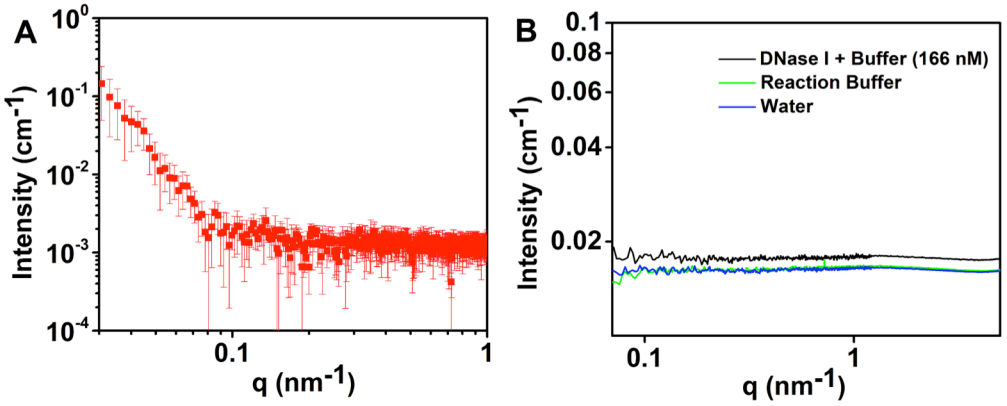

Figure S1: (A) Solvent subtracted SAXS intensity profile from DNase I (166.6 nM) (B) SAXS intensity profiles from pure water (blue), reaction buffer (green) and 166.6 nM DNase I dispersed in the reaction buffer (black).

S2. Effect of DNase I on native Catalase

While single-stranded DNA, double-stranded DNA and RNA are all known to be substrates for DNase I, this enzyme has not been reported to chemically modify or denature the *Cg* Catalase protein. To verify this, we measured the SAXS intensity profiles from the *Cg* Catalase protein before and after 2h incubation with 166.6 nM DNase I. The two intensity profiles were identical (Fig. S2), confirming that DNase I does not alter the native conformation of *Cg* Catalase.

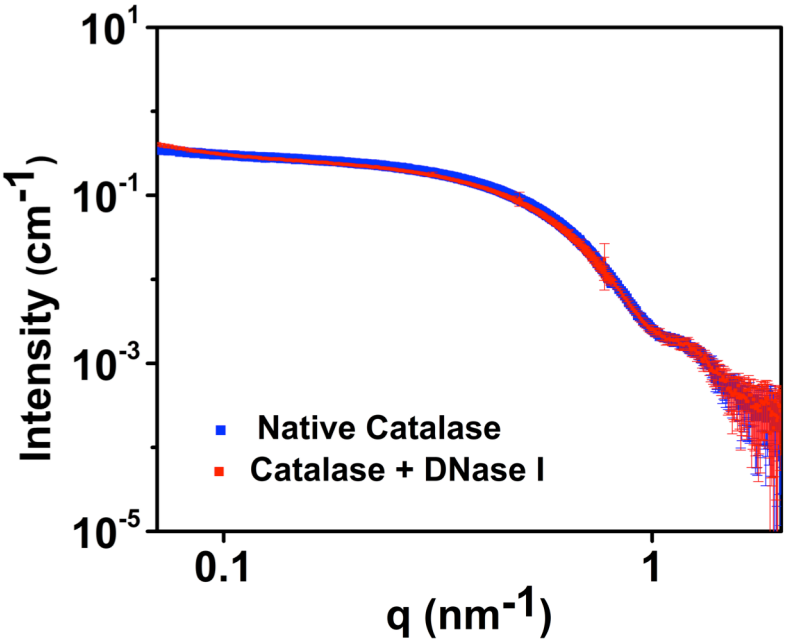

Figure S2: Background subtracted SAXS profiles from native Catalase before (blue) and 2h after (red) incubation with 166.6 nM DNase I, showing no appreciable changes.

S3. Forward scattering intensities from intact and degraded Pro-SNA

For a system of particles at dilute concentrations, the X-ray scattered intensity on the absolute scale (scattering cross-section per unit volume) can be written as:

$$I(q) = \frac{N}{V} r_e{}^2 \langle F(\vec{q})^2 \rangle_\Omega = \frac{N}{V} r_e{}^2 \langle \left| \int_{V_p} [\rho_p(\vec{r}) - \rho_s] e^{i\vec{q}.\vec{r}} dV_p \right|^2 \rangle_\Omega \quad \text{(S1)}.$$

Here, *N/V* is the particle concentration, r_e is the classical electron radius, $\vec{q}$ is the scattering vector, $F(\vec{q})$ is the particle form factor, which is equal to the Fourier transform of the particle's excess electron density $[\rho_p(\vec{r}) - \rho_s]$ above the electron density for the solvent, V_p is the volume of a single particle and the averaging in Eq. S1 is over all orientations of the particle.

For simplicity in the following analysis on the forward scattered intensities from Pro-SNA, we ignore the linker strands that connect the DNA to the protein core. Under this assumption, the scattered intensity from intact Pro-SNA can be written as:

$$I_{in}(q) = \frac{N}{V} r_e{}^2 \langle \left| \int_{V_{prot}} [\rho_{prot}(\vec{r}) - \rho_s] e^{i\vec{q}.\vec{r}} dV_{prot} + \sum_{j=1}^{N_{DNA}} e^{i\vec{q}.\vec{R}_j} \int_{V_j} [\rho_j(\vec{r'}) - \rho_s] e^{i\vec{q}.\vec{r'}} dV_j \right|^2 \rangle_\Omega \quad \text{(S2)}$$

Here, N_{DNA} is the number of DNA per Pro-SNA, $[\rho_{prot}(\vec{r}), \rho_j(\vec{r})]$ are the electron densities for the protein and the j^{th} DNA. The origins for the spatial coordinates in the two integrals in Eq. S2 are the centers of the protein and the j^{th} DNA. $\vec{R}_j$ represents the displacement of the center of the *jth* DNA from the center of the protein. From Eq. S2 the forward scattered intensity $I_{in}(q = 0)$ for intact Pro-SNA is

$$I_{in}(q = 0) = \frac{N}{V} r_e{}^2 [(\langle \rho_{prot} \rangle_r - \rho_s) V_{prot} + N_{DNA} (\langle \rho_{DNA} \rangle_r - \rho_s) V_{DNA}]^2 \quad \text{(S3)}.$$

Here, $(\langle \rho_{prot} \rangle_r, \langle \rho_{DNA} \rangle_r)$ are the average electron densities for the protein and the DNA, respectively.

Eq. S1 implies that at dilute concentrations, the total scattered intensity is the incoherent sum of the scattered intensities from distinct particles in the solution. Therefore, the scattered intensity from a solution containing degraded Pro-SNA is

$$I_{de}(q) =$$

$$\frac{N}{V} {r_e}^2 \langle \left| \int_{V_{prot}} [\rho_{prot}(\vec{r}) - \rho_s] e^{i\vec{q}.\vec{r}} dV_{prot} \right|^2 \rangle_\Omega + \frac{N \times N_{DNA} \times N_f}{V} {r_e}^2 \langle \left| \int_{V_f} [\rho_{DNA}(\overrightarrow{r'}) - \rho_s] e^{i\vec{q}.\overrightarrow{r'}} dV_f \right|^2 \rangle_\Omega \quad \text{(S4)}.$$

Here, N_f is the average number of fragments that each DNA is divided into and $V_f = V_{DNA}/N_f$ is volume of each of these DNA fragments. From Eq. S4, the forward scattered intensity from a solution containing degraded Pro-SNA and DNA fragments is:

$$I_{de}(q = 0) = \frac{N}{V} {r_e}^2 ([\big(\langle \rho_{prot} \rangle_r - \rho_s\big) V_{prot}]^2 + N_{DNA} \times N_f [(\langle \rho_{DNA} \rangle_r - \rho_s) \frac{V_{DNA}}{N_f}]^2) \qquad \text{(S5)}.$$

S4. The Two-State Model: Linear Combination Fitting

Fig. S3 shows examples of time-dependent scattered intensity profiles from 4 μM Pro-SNA incubated with 166.6 nM DNase I along with fits based on the two-state model (Eq. 3, main text). Each fit was performed by optimizing the time-dependent fraction of Pro-SNA in intact form [$\alpha(t) < 1$]. In these fits, the intensity profiles measured at t = 6 h was taken to correspond to pure state B (fully degraded Pro-SNA) because this scattered intensity profiles remained invariant over an additional 2 h of incubation of Pro-SNA with DNase I. A good match between the data and the fits verified the two-state model. Table S1 enumerates the fraction of Pro-SNA in intact (state A) and degraded (state B) states as a function of time for the dataset shown in Fig. 2A in the main text.

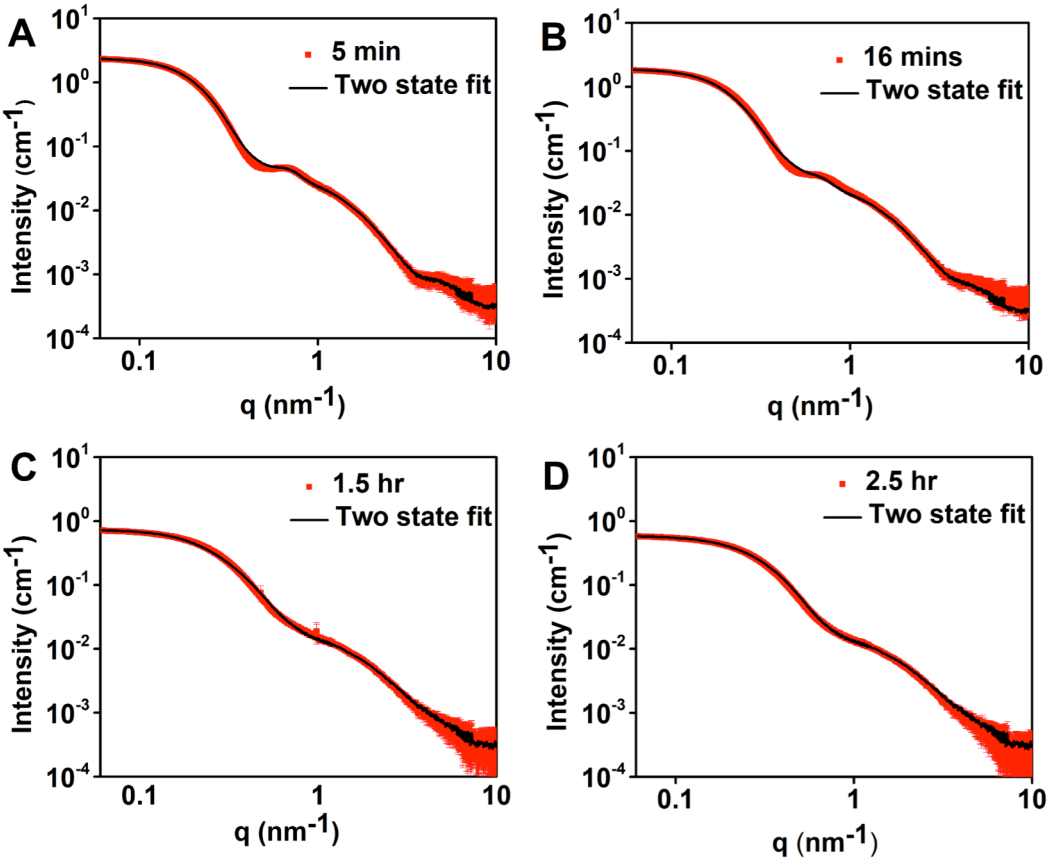

Figure S3: Examples of SAXS profiles measured from the Pro-SNA-DNase I system at 4 intermediate time points: 5 minutes (A), 16 minutes (B), 1.5 hours (C) and 2.5 hours (D) along with fits (black) based on Eq. 3.

Reaction time point	Fraction in State A (α)	Fraction in State B (1- α)
5 min	0.71	0.29
16 min	0.53	0.47
27 min	0.35	0.65
42 min	0.24	0.76
54 min	0.21	0.79
1.5 hrs.	0.09	0.91
2.5 hrs.	0.03	0.97

Table S1. Fraction of Pro-SNAs in State A (α) and State B (1- α) as a function of time.

S5. Time-dependent X-ray scattering for varied Pro-SNA concentrations

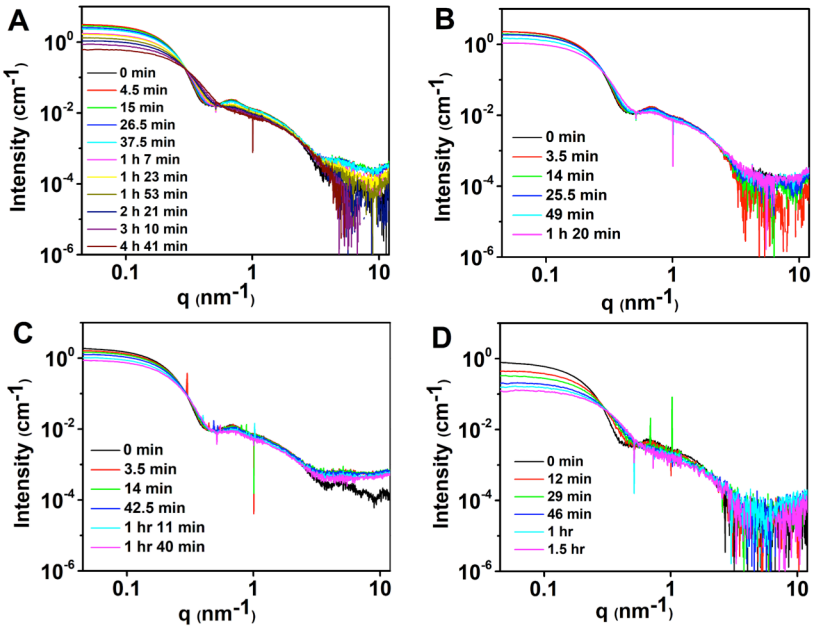

Figure S4: Background subtracted SAXS intensity profiles from Pro-SNA-DNase I systems as a function of reaction time for 2 μM Pro-SNA (A), 1.5 μM Pro-SNA (B), 1.0 μM Pro-SNA (C) and 0.5 μM Pro-SNA at a fixed DNase I concentration (43 nM).

Fig. S4 shows the time-dependent scattered intensity profiles from 2, 1.5, 1 and 0.5 μM Pro-SNA incubated with 43 nM DNase I. We note that due to limited time at synchrotron, the data for 1.5, 1.0 and 0.5 μM Pro-SNA was collected over ~ 1.5 h. In this time frame, the DNAse I-mediated degradation of Pro-SNA had not completed. For these sample sets, the scattered intensity profile corresponding to state B (degraded Pro-SNA) $I_B(q)$ was deduced by scaling down (based on concentration) the $I_B(q)$ for 4 μM Pro-SNA sample, measured at ~ 2.5 h.

S6. Ellipsoid model for protein

S6.1: Axes dimensions

Based on the atomic-scale structure for the *Cg* Catalase protein (PDB ID: 4B7F), the radii of gyration for the protein about the three orthogonal x, y, and z axes are 2.8, 3.2 and 2.7 nm, respectively.[1] For capturing the anisotropy in the protein shape, we modeled it as a homogenous ellipsoid. For this case, the calculated radii of gyration yield a = 4.9, b = 3.5 and c = 5.2 nm for the ellipsoid's semi axes. Since this ellipsoid is nearly a spheroid, for simplicity, we assumed $a' = c' = \sqrt{ac}$ = 5.05 nm. A 90° rotation about the x-axis leads to an ellipsoid with $a' = b'$ = 5.05 and c' = 3.5 nm, as depicted in Fig. 4A.

S6.2: Protein electron density

The average electron density for protein (ρ_{prot} = 403 e^-/nm^3) was obtained by fitting the measured SAXS intensity profile from 4 μM *Cg* Catalase in CRYSOL software,[2] which utilized the atomic scale structure of the *Cg* Catalase. The fit is shown in Fig. S5A in our previous publication.[1]

S7. MALDI mass spectrometry of reaction products

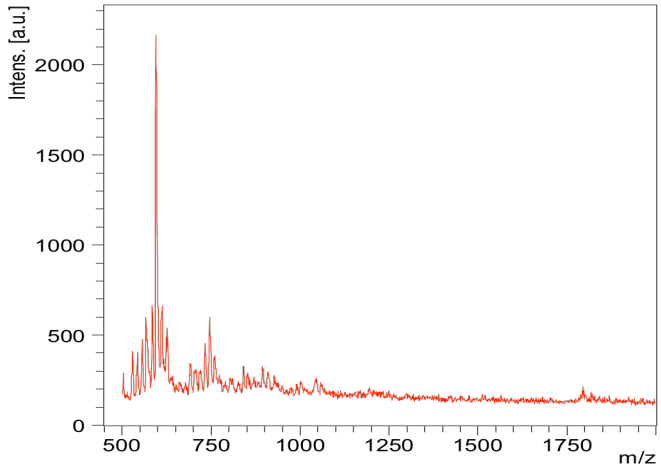

Figure S5: MALDI Mass spectrum collected from the DNA products of the enzymatic degradation reaction.

To identify the products of the degradation of the DNA on a Pro-SNA by DNase I, we used MALDI-TOF mass spectrometry. Pro-SNA (4 μM) was incubated with DNase I (332 nM) for 2 h at room temperature. The degraded DNA products were isolated from the Pro-SNA and DNase I by ultracentrifugation using Amicon Ultra 30 kDa spin filters. The run-off was collected, mixed with 2',4'- DHAP MALDI matrix and deposited on a MALDI plate. The sample was then analyzed using MALDI-TOF mass spectrometry on a Bruker AutoFlex spectrometer. The resultant mass spectrum (Fig. S5) displays a dominant peak corresponding to a mass of 594 Da (assuming a charge Z = 1 for the ionized molecules). This is roughly equivalent to the mass of two DNA bases. Additional weaker peaks corresponding to fragments with higher masses (tri-nucleotides) are also observed. The mass spectrometry data provides qualitative confirmation of the X-ray scattering-derived result that the degraded DNA disperse in the solution as small fragments. However, the X-ray analysis shows that the fragments are 3 base pairs long. A possible reason for this discrepancy is discussed in the next section *S8.3*.

S8. Pro-SNA simulations

S8.1: Cylindrical model for DNA

Here, we discuss the parameters used for the DNA in model calculations.

S8.1.1 Length of the DNA: Pair distance distribution function (PDDF) analysis

In order to gain model-independent insight into the extension of DNA shell on Pro-SNA, we performed PDDF analysis[3] on the measured SAXS intensities. The PDDF function $P(r)$ is given by

$$P(r) = r^2\gamma(r) = \frac{r^2}{2\pi^2}\int_0^\infty q^2 I(q)\frac{\sin(qr)}{qr}dq \quad \text{(S6)}.$$

Here, $\gamma(r)$ is the orientationally-averaged auto-correlation function of the particle's electron density, and $I(q)$ is the measured scattered intensity profile from a dilute solution of particles. From Eq. S6, $P(r) = 0$ when $r = 0$ and when $\gamma(r) = 0$, which occurs for $r \geq D_{max}$, the maximum dimension of the particle.

PDDF analysis (Fig. S6) shows that the D_{max} of the intact Pro-SNA is ~ 10 nm greater than that for the degraded Pro-SNA. This is consistent with the DNA length of 5 nm in our model calculations. We do note that this DNA length is less than the expected length of ~ 6.4 nm for a 20 base-pair long double stranded (ds-) DNA in B-DNA conformation. We speculate that this difference is likely because, in reality, DNA have a range of tilts with respect to protein's surface normal. Such tilting might be facilitated by the flexible linkers, which couple the protein to the DNA.

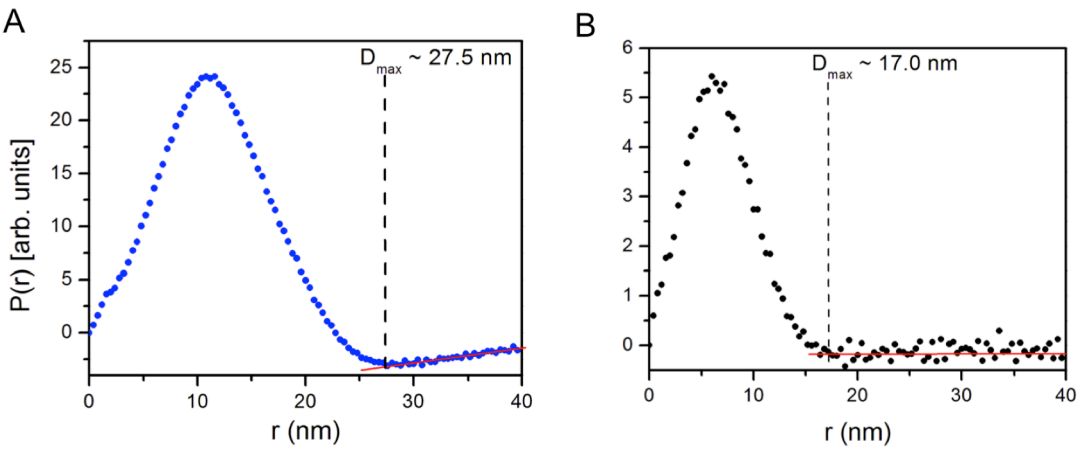

Figure S6: Pair distance distribution functions calculated for intact Pro-SNA (blue) and degraded Pro-SNA (black). Data over a range $0.03 \leq q \leq 10$ nm^{-1} was used to compute the Fourier transform in Eq. S6.

S8.1.2. Radius of the DNA.

The diameter of the double stranded DNA was chosen to be D = 2.0 nm, consistent with previous SAXS studies.[4] From the perspective of X-ray scattering, the cylindrical DNA model results in a modulation in the scattered intensity profile with a minimum at q_{min} = 3.8/R = 3.8 nm^{-1}. This modulation with q_{min} = 3.8 nm^{-1} is clearly observed in the experimental SAXS profile from intact Pro-SNA (Fig. 3C, main text), validating the DNA diameter value used in the simulations.

S8.1.3. DNA electron density.

The electron density for the double-stranded DNA is known to be ρ_{DNA} ~ 550 e-/nm^3.[4] By contrast, in our simulations, we have used ρ_{DNA} ~ 440 e-/nm^3. This lowered value of the electron density arises likely because 1). The volume of the DNA in the cylindrical model is greater than the actual DNA volume, 2) all the DNA on a Pro-SNA are not in their duplexed form. Based on our previous study on DNA-coated Au nanoparticles,[5] we expect that about 60 -

70% of the DNA are in the duplexed form, and 3) the total number of DNA on a Pro-SNA may not be N_{DNA} = 40 the mean value derived from UV-VIS measurements, which typically have a ± 20% associated uncertainty. In Fig. S7, we show that tweaking the DNA electron density or the number of DNA can account for the discrepancy between the MALDI results and the simulation of X-ray scattered intensities in the size of the degraded DNA fragments.

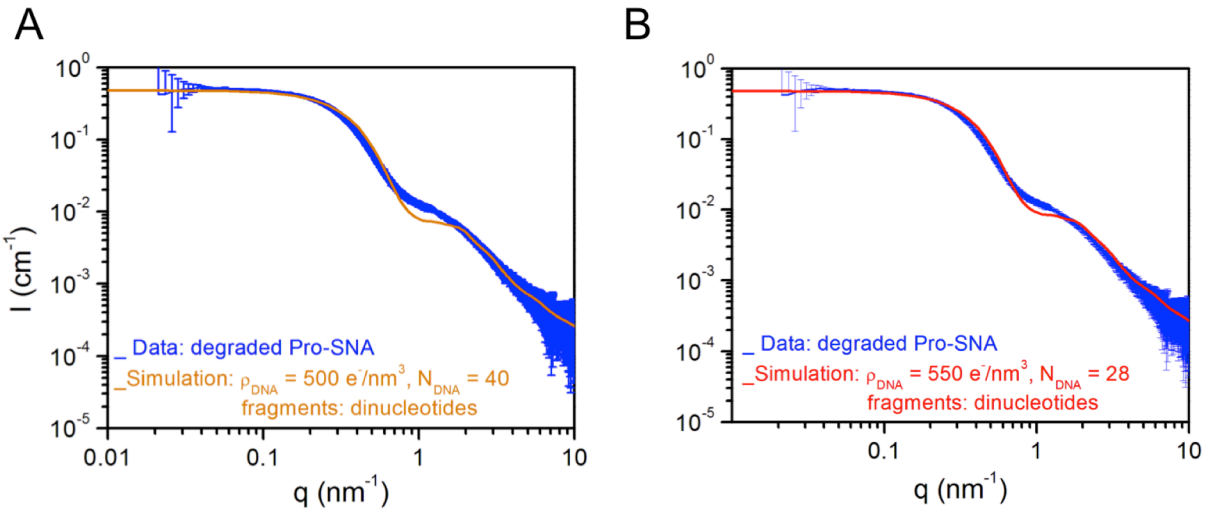

Figure S7: (A) Scattered intensity profile from solutions containing degraded Pro-SNA along with simulated intensity profiles based on (A) ρ_{DNA} = 500 e$^-$/nm^3, N_{DNA} = 40 and (B) ρ_{DNA} = 550 e$^-$/nm^3, N_{DNA} = 28. In both the simulations, the length of the degraded DNA fragments is 0.34 nm, corresponding to 1 base-pair of ds-DNA in B-conformation, and the parameters for the protein and the linkers are the same as those described in the main text.

S8.2: SAXS profile from intact Pro-SNA (State A)

Here we discuss the structural origins of the intensity modulations in the SAXS intensity profile for intact Pro-SNA (Fig. 1B, 2A and 4C, main text). For this, we simulate the scattered intensity profile for intact Pro-SNA as a function of DNA grafting density (Fig. S8A) and DNA length (Fig. S8B). In all these simulations, the positions of the DNA attachment sites on the ellipsoid, which represents the protein, were obtained by solving numerically the Thomson

problem, as described in the main text. The parameters for the protein and linker, as well as the DNA electron density and radius were held fixed to the values noted in the main text.

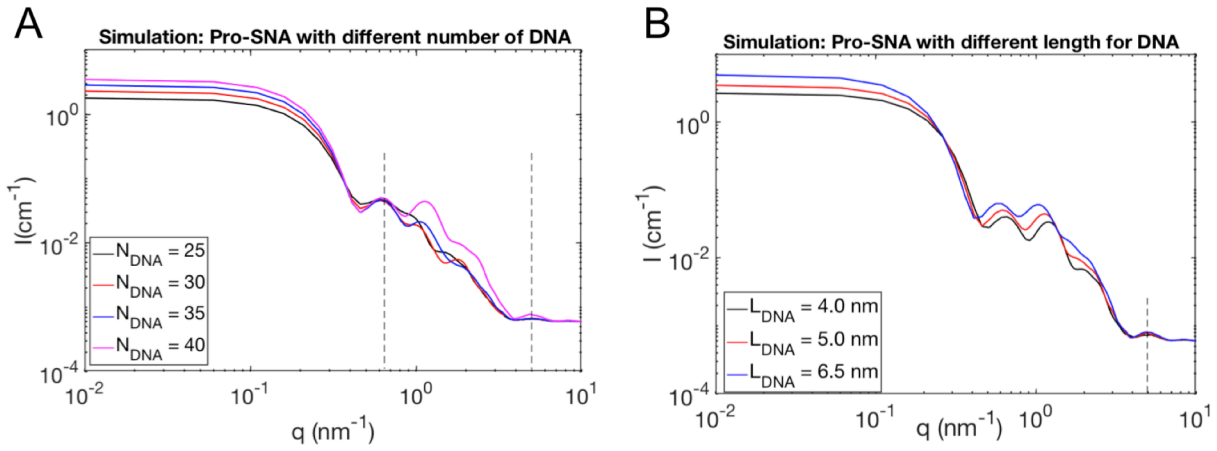

Figure S8: Simulated intensity profiles for 4 μM intact Pro-SNA dispersed in water for (A) different number of DNA (N_{DNA}) per protein and (B) different lengths of the DNA (L_{DNA}).

Based on the two sets of calculations in Fig. S8, the following conclusions can be drawn:

1. The position of the maximum in the region $0.6 < q_{max,1} < 0.7$ nm^{-1} depends sensitively on the DNA length (Fig. S8B), but not on the DNA loading density (Fig. S8A). In particular, $q_{max,1} \sim 2\pi/(L_{Linker} + L_{DNA})$. Here, L_{Linker} and L_{DNA} are the lengths of the linker and the DNA. This implies that this intensity modulation is due to the spatial extent of the compound linker + DNA construct, and not due to the positional correlations between the DNA on the protein surface. We note that a calculation based on $L_{Linker} + L_{DNA} = 9$ nm reproduces, approximately, the observed amplitude and position of this intensity modulation (Fig. 4C, main text).
2. The position of the local maximum $q_{max,2}$ near 1 nm^{-1} shifts to a lower q with decreasing DNA loading density (or increasing average interDNA separation) as well as with increasing DNA length. We note that the position of this modulation in the measured SAXS profile is approximately reproduced with $L_{Link} + L_{DNA} = 9$ nm and $N_{DNA} = 40$, but the

modulation is smeared out in the experimental data. This difference between experiment and calculation is due to the simplicity of the model. For example, there maybe a wide distribution of interDNA separations on the Pro-SNA. In particular, the relatively regular arrangement of the attachment sites obtained from solving the Thomson problem cannot be expected to exactly match the position of lysines on the protein surface, where the linker + DNA are covalently bound.

3. The position of the local maximum at $q_{max,3}$ ~ 5 nm^{-1} is due to the DNA cross-section, and is therefore independent of the DNA length or the DNA loading density on the Pro-SNA.

S8.3: SAXS profile from degraded Pro-SNA (State B)

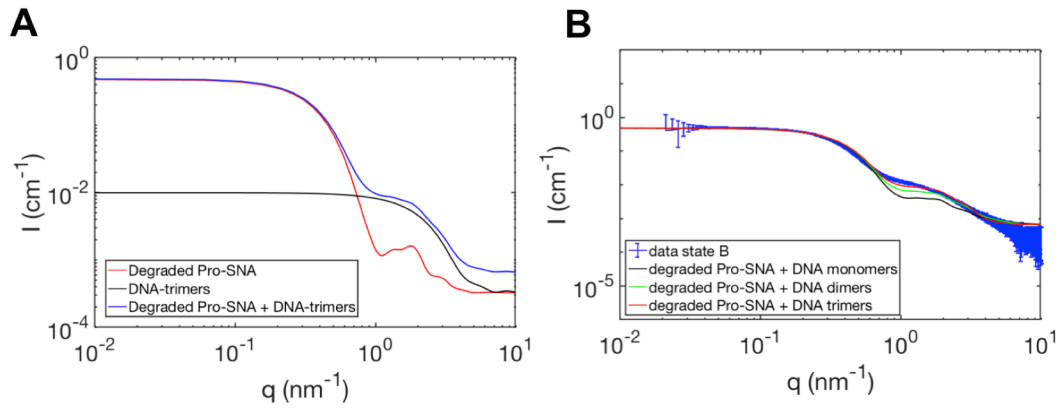

Figure S9: (A) Simulated intensity profiles showing the combined scattering (state B, blue) from 4 μM degraded Pro-SNA and the corresponding degraded DNA trimers. The individual scattering contributions from the degraded Pro-SNA (red) and the DNA trimers (black) are also shown. (B) Comparison between the measured, background-corrected scattering from degraded Pro-SNA and the degraded DNA (state B) with simulations for the cases where the degraded DNA are 1 (black), 2 (green) and 3 (red) base-pair long. In all the simulations, the number of DNA base-pairs (800/protein) are identical. The parameters for the protein, linker as well as the DNA electron density and radius were held fixed to values described in the main text.

S9. Molecular dynamics simulation

S9.1: Method

The molecular dynamics simulations were performed in HOOMD-blue[6, 7] version 2.1.5 on GPU using a Langevin integrator[8] ($\lambda = 1.9 \times 10^{-5}$ Pa·s) at 293 K with a timestep of 5 fs for a total of 100 ns. To allow for equilibration, only the last 75 ns were used for analysis. The simulation consisted of one Pro-SNA complex in a square box of side length 74.607 nm, corresponding to the average Pro-SNA concentration of 4 μM. Solvent is represented implicitly (with a uniform relative dielectric constant of 78) and ions are represented explicitly. The parameters for the coarse-grained model for the Pro-SNA and explicit ions are listed in Table S2. A snapshot of the system mid-simulation is given in Fig. S10, and a clip of the simulation is given in the accompanying movie. In both, some ions in the bulk solution are not represented for clarity.

Pro-SNA: The full Pro-SNA complex consists of one protein covalently bonded to 40 chains of linker each coupled to 20 base pair long double-stranded DNA strands. The protein was modelled as an ellipsoid with axes $a = b = 5.05$ nm, $c = 3.5$ nm and was represented forming a surface of 4,358 beads of 0.2 nm radius. Attachment sites for the 40 linker-DNA chains were selected from the surface beads using a numerical solution to the ellipsoidal extension of the Thomson problem, as described in the Results and Discussion section (main text).

Each of the 40 attached chains included a linker section (connected to protein and DNA) and a double-stranded DNA section. The linker section was a flexible chain consisting of 10 linker beads (properties listed in Table S2) connected by harmonic bonds and no additional angle or dihedral potentials. Because each linker carries a charge of -3 e^-, the 10 linker beads were assigned a charge of -0.3 e.

The double-stranded DNA portion of each chain was represented by 10 coarse-grained beads, each bead representing two base pairs of DNA. The radius of the DNA beads was 1.0 nm, so the diameter of the DNA strand was 2.0 nm. The equilibrium length of the DNA bead-DNA bead bonds (also harmonic) was chosen so that the DNA strand would have an average rise per base pair of ~ 0.33 nm, consistent with B-conformation of ds-DNA (see Table S3 for bond parameters). Harmonic angle potentials were applied to the DNA strand; see Table S4. Though the DNA portion of each strand is stiff, the flexibility of the linker allows the DNA to rotate somewhat freely.

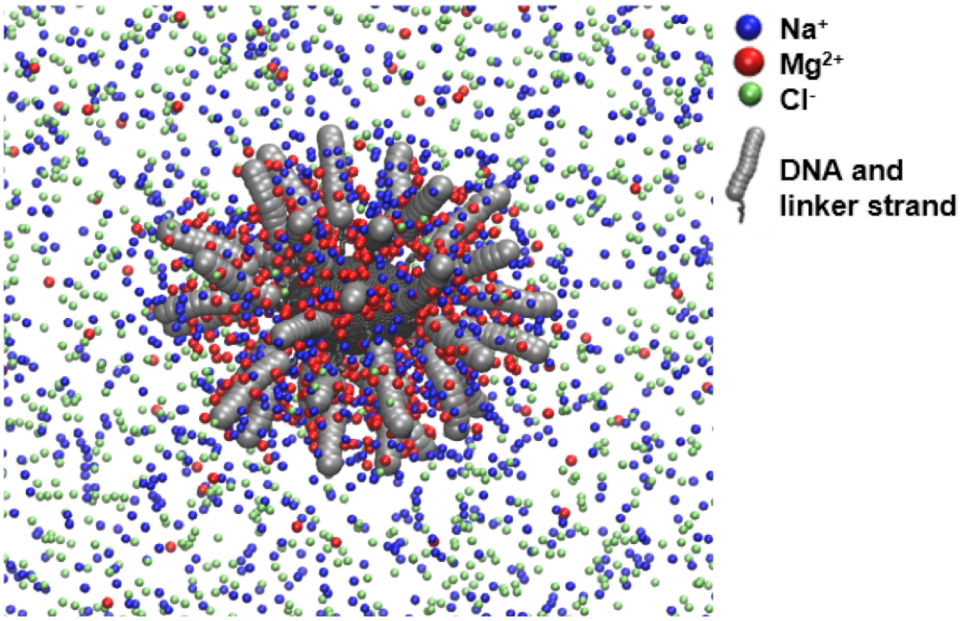

Figure S10: Model of the Pro-SNA as represented in the MD simulations. The correspondence between bead color and the object type is: silver: DNA, red: divalent cation, blue: monovalent cation, green: anion, black: nanoparticle surface and linker.

Ions: Ions in the system were represented explicitly using coarse-grained beads. Although the solution included two species of monovalent cation and two species of divalent cation, we simplified this system by representing all monovalent cations with the properties of Na^+, all divalent cations with the properties of Mg^{2+}, and all anions with the properties of Cl^-, as described in the Results and Discussion section. The dimensions in Table S2 were taken from SI ref. 9. Also, as described in the Results and Discussion section, monovalent cations were added as counterions to neutralize the total negative charge from the Pro-SNA (6.88 mM), then 7.52 mM NaCl and 3 mM $MgCl_2$ were added to the resulting system.

General: The non-bonded interactions between beads consisted of the soft-core excluded volume interactions (WCA potential[10]) between all species, and electrostatic interaction between the charged species (calculated using the PPPM method[11] implemented in HOOMD-blue).

Because the goal of the MD simulation is to understand the ion distribution around the Pro-SNA, the motion of the protein itself was not important to calculate. Therefore, during the integration, all components except the particles directly representing the protein were integrated.

Bead type	**Radius (nm)**	**Charge (e)**	**Num. beads per chain**
Linker	0.175	-0.3	10
Double-stranded DNA (2 base pairs)	1.0	-4	10
Monovalent cation (Na^+)	0.358	+1	*N/A*
Divalent cation (Mg^{2+})	0.428	+2	*N/A*
Anion (Cl^-)	0.332	-1	*N/A*

Table S2. Properties of coarse-grained beads and electrolyte ions in the MD simulation.

Bond type	**r_0 (nm)**	**k_r (k_BT)**
Linker-linker	0.35	75
Linker-DNA	0.33	75
DNA-DNA	0.66	300

Table S3. Bond parameters, corresponding to the harmonic potential $V(r) = \frac{1}{2}k_r(r - r_0)^2$

Angle type	θ_0 (rad)	k_θ (k_BT)
Linker-linker-linker	π	0.0
Linker-linker-DNA	π	0.0
Linker-DNA-DNA	π	63
DNA-DNA-DNA	π	63

Table S4. Angle parameters, corresponding to the harmonic potential $V(\theta) = \frac{1}{2}k_\theta(\theta - \theta_0)^2$

S9.2: Ion distribution surrounding DNA chains in Pro-SNA

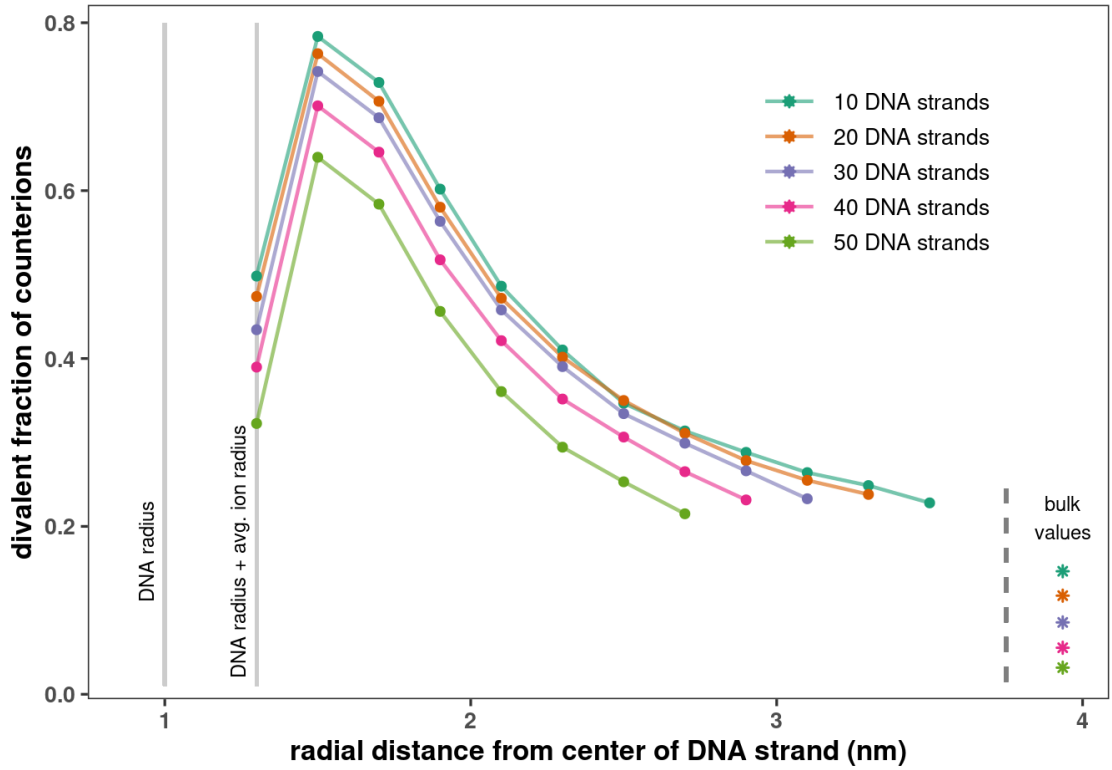

Figure S11: Fraction of counterions that are divalent as a function of distance from the axis of DNA strands for varied DNA loading densities on the Pro-SNA. These estimates are averaged over all DNA strands of the Pro-SNA and over all equilibrated frames. The input concentrations of monovalent and divalent cations are the same in each run (14.4 mM and 3.0 mM, respectively). Because of the difference in total number of DNA strands present (*i.e.* total Pro-SNA charge to be compensated), the final bulk ionic concentrations differ; these are indicated on the plot (bottom, right). The data for each simulation is cut off at a distance corresponding roughly to half of the average distance between neighboring DNA strands.

Figure S11 shows MD-simulations derived estimates for the fraction of total counterions that are divalent [N_{Mg}^{2+}/ (N_{Mg}^{2+} + N_{Na}^{+})] as a function of distance from the center of the DNA strand in a direction normal to the DNA axis. For Pro-SNA with 40 DNA strands (discussed in the paper), in the neighborhood of the DNA strand, ~ 70% of the condensed counterions are divalent. This is considerably higher than the average value of 52% for the divalent cations in the DNA shell. This reveals the role of spatially varying electrostatic potential on the non-uniform distribution of counterions in the DNA shell. Furthermore, with decreasing DNA loading, the fraction of divalent ions in this condensed layer monotonically increases. This should be a consequence of the coupling between the variation in electrostatic potential as a function of the DNA loading density and the fact that there are proportionally more divalent ions available in the bulk solution to satisfy the requirement of uniform electrochemical potential. Namely, $Z\psi(\vec{r}) + k_B T ln[n(\vec{r})] = k_B T ln[n_b]$. Here, *Z* is the ionic charge, $\psi(\vec{r})$ is the electrostatic potential at a specific location $\vec{r}$ and $n(\vec{r})$ and n_b are the ion number density at a specific location and in the bulk solution, respectively. Our future work on combining ASAXS with simulations will shed more light on this important conceptual issue.

REFERENCES

1. Krishnamoorthy, K.; Hoffmann, K.; Kewalramani, S.; Brodin, J. D.; Moreau, L. M.; Mirkin, C. A.; Olvera de la Cruz, M.; Bedzyk, M. J. Defining the Structure of a Protein-Spherical Nucleic Acid Conjugate and Its Counterionic Cloud. *ACS Cent. Sci.* **2018,** *4*, 378-386.
2. Svergun, D.; Barberato, C.; Koch, M. H. J. Crysol - a Program to Evaluate X-Ray Solution Scattering of Biological Macromolecules from Atomic Coordinates. *J. Appl. Crystallogr.* **1995,** *28*, 768-773.
3. Svergun, D. I.; Koch, M. H. J. Small-Angle Scattering Studies of Biological Macromolecules in Solution. *Rep. Prog. Phys.* **2003,** *66*, 1735-1782.
4. Tokuda, J. M.; Pabit, S. A.; Pollack, L. Protein-DNA and Ion-DNA Interactions Revealed through Contrast Variation SAXS. *Biophys. Rev.* **2016,** *8*, 139-149.

5. Kewalramani, S.; Guerrero-Garcia, G. I.; Moreau, L. M.; Zwanikken, J. W.; Mirkin, C. A.; Olvera de la Cruz, M.; Bedzyk, M. J. Electrolyte-Mediated Assembly of Charged Nanoparticles. *ACS Cent. Sci.* **2016,** *2*, 219-224.

6. Anderson, J. A.; Lorenz, C. D.; Travesset, A. General Purpose Molecular Dynamics Simulations Fully Implemented on Graphics Processing Units. *J. Comput. Phys.* **2008,** *227*, 5342-5359.

7. Glaser, J.; Nguyen, T. D.; Anderson, J. A.; Lui, P.; Spiga, F.; Millan, J. A.; Morse, D. C.; Glotzer, S. C. Strong Scaling of General-Purpose Molecular Dynamics Simulations on Gpus. *Comput. Phys. Commun.* **2015,** *192*, 97-107.

8. Phillips, C. L.; Anderson, J. A.; Glotzer, S. C. Pseudo-Random Number Generation for Brownian Dynamics and Dissipative Particle Dynamics Simulations on Gpu Devices. *J. Comput. Phys.* **2011,** *230*, 7191-7201.

9. Dove, P. M.; Nix, C. J. The Influence of the Alkaline Earth Cations, Magnesium, Calcium, and Barium on the Dissolution Kinetics of Quartz. *Geochim. Cosmochim. Acta* **1997,** *61*, 3329-3340.

10. Weeks, J. D.; Chandler, D.; Andersen, H. C. Role of Repulsive Forces in Determining Equilibrium Structure of Simple Liquids. *J. Chem. Phys.* **1971,** *54*, 5237-5247.

11. LeBard, D. N.; Levine, B. G.; Mertmann, P.; Barr, S. A.; Jusufi, A.; Sanders, S.; Klein, M. L.; Panagiotopoulos, A. Z. Self-Assembly of Coarse-Grained Ionic Surfactants Accelerated by Graphics Processing Units. *Soft Matter* **2012,** *8*, 2385-2397.